

Peng QIAN, Peng FENG, Lieping YE

# Experimental study on GFRP pipes under axial compression

© Higher Education Press and Springer-Verlag 2008

**Abstract** Fiber reinforced polymer (FRP) is suitable for structures in corrosive environment and long-span light-weight structures due to its high-strength, light-weight, and anti-corrosive qualities. The behavior of pultruded glass fiber reinforced polymer (GFRP) pipes, which are the members of long-span lattice structures, under axial compression was investigated by tests. Short GFRP pipes were first tested to determine the basic mechanical properties. Then the stability of long GFRP pipes was studied by axially compressive tests in four groups with different slenderness ratios, twelve specimens totally. Based on the results of the tests and literature, the formula of the buckling load of composite pipes under axially compressive load was presented based on Perry formula. It can well predict the buckling failure load GFRP pipe under axial compression.

**Keywords** stability, buckling, corrosion resistance, long-span structure, light-weight structure

## 1 Introduction

Fiber reinforced polymer (FRP) has been promoted and applied gradually in various fields of the modern engineering since the 1940s due to its characteristic of high-strength, high-modulus ratio, and anti-corrosive. The price of FRPs has decreased for the progress of manufacturing technology and industrialization, which has brought more application in civil engineering structures since the 1970s [1,2]. GFRP (glass FRP), CFRP (carbon FRP), and AFRP (aramid FRP) are FRPs in common use, and GFRP is in the broadest application in engineering due to its reasonable price and larger ratio of elongation [2–4].

Translated from *Journal of Tianjin University*, 2007, 40(1): 19–23 [译自: 天津大学学报]

Peng QIAN, Peng FENG, Lieping YE (✉)  
MOE Key Laboratory of Structural Engineering and Vibration,  
Tsinghua University, Beijing 100084, China  
E-mail: fengpeng@tsinghua.edu.cn, ylp@tsinghua.edu.cn

FRP with the characteristic of light-weight and high-strength which is the ideal material to build long-span spatial structures can form lots of lattice structure such as grid and net shell. It has lots of advantages for building large-span special roof such as the good adjustability for structures, the ability to form variously shaped spatial curves, the convenience to transport and install, low-cost for maintenance, well-durability, short-construction cycle, and the ability to avoid corrosion induced by rain and dew. The behavior of pultruded GFRP pipes, which are the members of spatial grid structure, under axial compression was investigated in tests. The axial bearing capacity and basic material parameters of the GFRP pipes were first obtained through short-pipe compressive test; then long pipes under axial compression were tested to study the relations between its stability and slenderness ratio and its instability failure modes; the approach to calculate the buckling load of under axially compressed pipes is presented on the basis of study and summarization of the result of the test and literature.

## 2 Short pipes strength tests

The tested GFRP pipes made from E-glass fiber and vinyl resin was produced by pultrusion, with circle section with external diameter of 41.2 mm and thickness of 3.6 mm. Axially compressive tests to short pipes with length of 120 mm were processed to obtain material properties and the axially compressive strength. Five specimens were taken from different batches of the GFRP pipe products. The GFRP pipes were exerted axial pressure after alignment on compressive test machine as the testing setup shown in Fig. 1. Two groups of strain gauges with two crossing sheets were placed in the opposed places of the central section of the outer-surface of the pipes to measure the axial strain and transverse strain of the GFRP pipes.

The relations of the load and strain measured during the progression of the tests were linear in the gross. A sound of “pipa” was caught when the longitudinal strain reached to 5000  $\mu\epsilon$ , and the sound continued to the destruction of the pipe. The longitudinal strain of the pipe reached to 6200  $\mu\epsilon$  to 7800  $\mu\epsilon$  when the specimens were

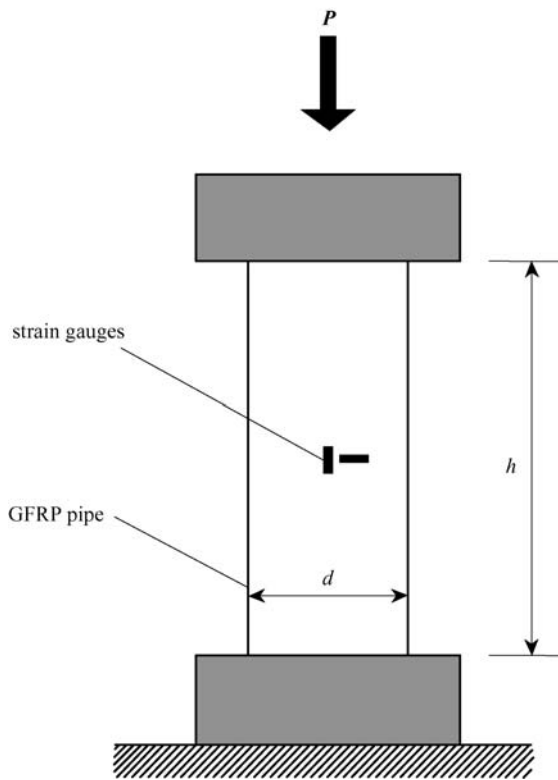


**Fig. 1** Testing setup for short GFRP pipes under axial compression

destroyed which was a sudden course comparatively and accompanied by huge noises. The destruction of the pipes was presented in Fig. 2, from which a number of longitudinal cracks on the surface of the GFRP pipes were emerged.



**Fig. 2** Failure mode of short GFRP pipes

The experimental results of short GFRP pipes under axial compression were presented in Table 1, in which the mechanical properties were taken from the average value of the pipes. The test result of SCGP-4 was discarded for obviously difference from the others. The elastic properties of the pultruded FRP pipes had little difference with a 5.5% variation coefficient from the result of the tests; and there was a large value of dispersion with the coefficient of variation of the ultimate load, longitudinal ultimate stress and strain was 10.9% and 10.5% respectively; the dispersion of toroidal ultimate strain was

larger, with a value of 20.3%, which was caused by the instability of the number and the distribution of the cracks of the sample approaching the destruction.

**Table 1** Experimental results of short GFRP pipes under axial compression

No.	$P_u$ /kN	$\varepsilon_{u,L}/\mu\varepsilon$	$\varepsilon_{u,T}/\mu\varepsilon$	$\sigma_{u,L}$ /MPa	$E_L$ /MPa	$\nu_{L,T}$
SCGP-1	92.0	7819	2936	216.4	27682	0.39
SCGP-2	71.0	6192	2178	166.8	27054	0.35
SCGP-3	87.0	7284	3463	204.4	28347	0.38
SCGP-4	73.0	6331	1709	171.6	21626	0.27
SCGP-5	87.0	7820	2480	204.4	26404	0.35
average	84.3	7279	2764	198.4	27372	0.37
coefficient of variation	10.9%	10.5%	20.3%	10.9%	3.0%	5.5%

Notes:  $P_u$  is the failure load of the pipes;  $\varepsilon_{u,L}$  and  $\varepsilon_{u,T}$  are the longitudinal and transverse average failure strains of the samples;  $\sigma_{u,L}$  is the longitudinal average failure stress of the pipes, named as ultimate strength;  $E_L$  and  $\nu_{L,T}$  are longitudinal modulus of elasticity and longitudinal and transverse Poisson's ratio respectively.

### 3 Long pipes stability tests

Four groups of GFRP pipes with the different slenderness ratios and the same cross-section as the tested short pipes, which include 3 specimens in each group and have 12 totally, were tested to investigate the stability of GFRP pipes under axial compression. Their parameters are shown in Table 2. The GFRP pipes were placed in the fixture (the valid calculated length of element includes the height of the fixture with two ends), then were exerted longitudinal pressure after alignment. Their longitudinal strain and lateral displacements of the middle section, and vertical displacement of the load end were measured, the testing setup and the placement of the strain gauge and displacement meters as shown in Figs. 3 and 4.

**Table 2** Geometrical parameters of tested long GFRP pipes

No.	length $l$ /mm	slenderness ratio	support condition
LCGP35	700	35	fixed ends
LCGP45	1000	45	fixed ends
LCGP55	1300	55	fixed ends
LCGP90	1500	90	fixed bottom/hinged top

Note: LCGP35 means Long Compressive GFRP Pipes 35 (slenderness ratio).

The tested specimens had the similar phenomenon in the gross: little deformation at the beginning of the loading; when it closed to buckling load, the lateral displacement in the central part of the bar increased rapidly; then the buckling of the whole element occurred. The lateral deformation of the pipes was in the shape of half-wave sine curve when it was instability. It belongs to overall buckling failure.

Figures 5–8 are the axial force- middle-point lateral displacement curves of all groups of specimens. It can

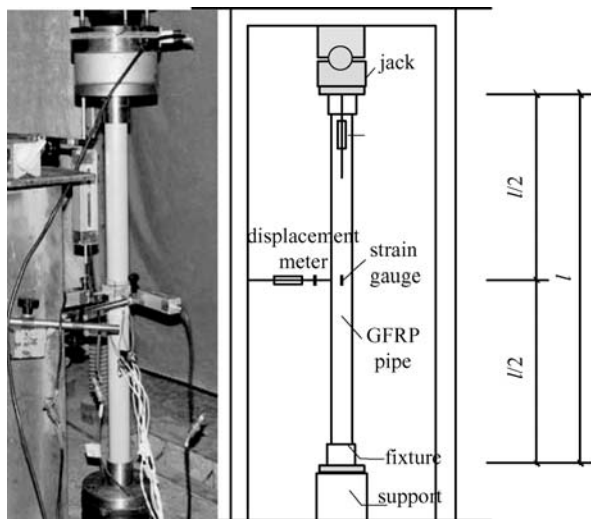


Fig. 3 Testing setup for long GFRP pipes under axial compression

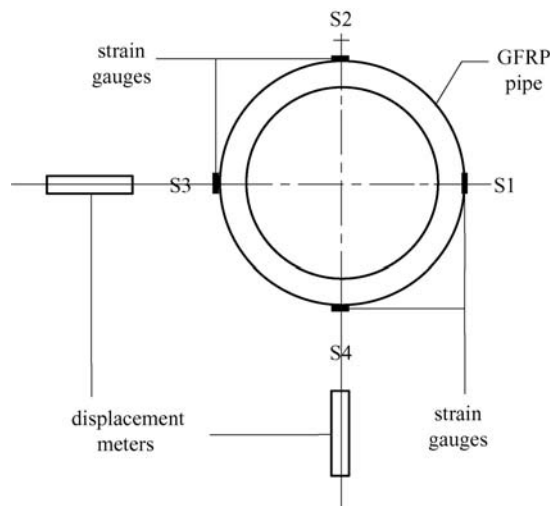


Fig. 4 Location of measured points in the middle section

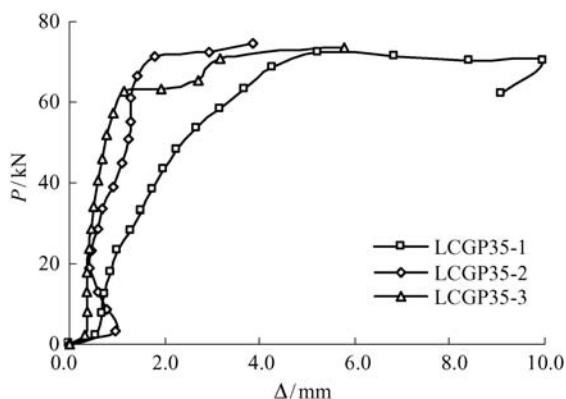


Fig. 5 Axial force-lateral displacement curves of LCGP 35

been seen in the curves that the existing of the initial defect leads the lateral displacement increasing with the load raising, and there appears a distinctive inflexion with the

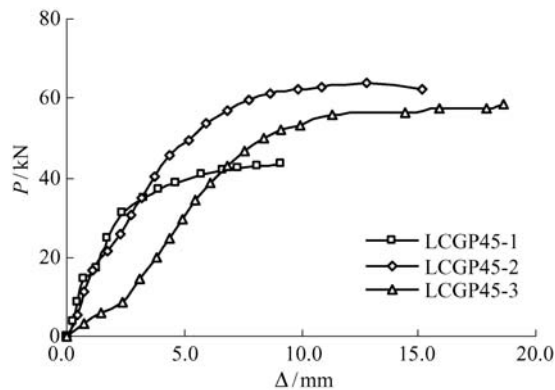


Fig. 6 Axial force-lateral displacement curves of LCGP 45

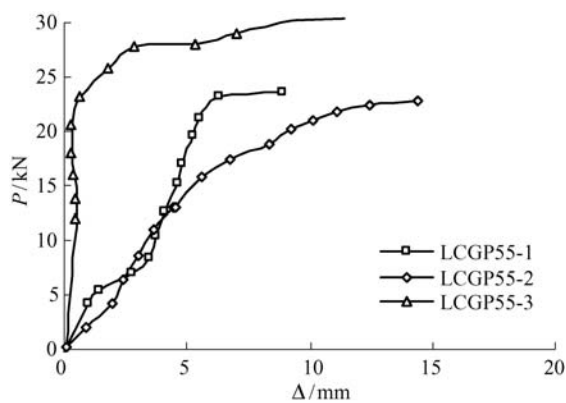


Fig. 7 Axial force-lateral displacement curves of LCGP 55

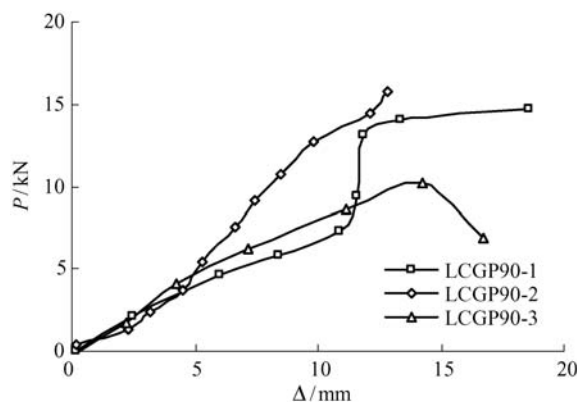


Fig. 8 Axial force-lateral displacement curves of LCGP 90

buckling, since then the vertical load nearly become invariable but the lateral deformation increases rapidly until the failure of the sample.

Figure 5 shows the axial force-lateral displacement curves of LCGP 35 group. As the existence of a small gap in the support bracket, there is an inflexion on the curves at the beginning of the loading. The lateral displacement of LCGP 35-1 and LCGP 35-3 increased rapidly after instability, and the specimens reached to

the ultimate compression and failure occurred when the lateral displacement reached to 10 mm; the LCGP 35-2 appeared failure soon after instability as the stress concentration near the end, and the lateral displacement was only 4 mm at this point.

Figure 6 shows the axial force-lateral displacement curves of LCGP 45 group. The lateral stiffness of LCGP 45-3 had an abrupt change because a contact slip happened when the load reached to 10 kN. The stiffness of three specimens kept homologous until the instability of the samples.

Among them, the buckling load of LCGP 45-1 was comparatively lower, 44 kN, as the inadequately end constraint caused by little rotation of the fixture, but the buckling loads of the other two were around 60 kN.

Figure 7 shows the axial force-lateral displacement curves of LCGP 55 group. The lateral stiffness of LCGP 55-3 increased slowly before its buckling, and it had the largest buckling load in the three specimens, which proved that its initial defect is comparatively small. Obviously, the initial defect is a very important factor to influence the buckling load of elements.

Figure 8 shows the axial force-lateral displacement curves of LCGP 90 group. When LCGP 90-1 was loaded to 8 kN, the ends of the bar were pressure-compacted partially, so its stiffness bounced suddenly, that is its lateral displacement kept constant while the axial load increased. To 13 kN, the lateral displacement increased suddenly, it went to the condition of instability quickly. Compared with LCGP 90-1, the stiffness of the other two specimens changed little during the loading.

#### 4 Overall stability analyses of GFRP pipes

There are a few of researches on the overall stability of GFRP members published in abroad while barely in domestic.

Goodman et al [5] tested three boron/epoxy FRP pipes with the radius of 81 mm and the thickness of 0.53 mm under axial compression. The ratio between the experimental results and the calculated result by the Euler formula are 0.81, 0.97 and 1.06 respectively. The elastic modulus  $E$  was determined by experiment of short column under axial compression. The Euler formula is

$$P_E = \frac{\pi^2 EI}{L^2}. \quad (1)$$

Hewson et al [6] investigated the flexural buckling, torsional buckling and flexural torsional coupling buckling of pultruded C-shaped GFRP members under axial compression. The flexural buckling load of the components was calculated by Euler formula, but  $E$  and  $G$  were replaced by longitudinal elastic modulus  $E_L$  determined

by bending test and longitudinal-transversal shear modulus  $G_{LT}$  determined through torsion test. The error of the buckling loads of experiment to the theoretical result was from 5% to 11%. Lee and Hewson [7] found that the shear deformation must be considered as  $E_L/G_{LT}$  was comparatively large based on the study on the buckling properties of the CFRP C-shaped members under axial compression in 1979. They suggested that the buckling load of slender FRP component should be calculated by the modified Euler formula as:

$$P_t = \frac{P_E}{1 + (P_E/K_s A_g G_{Lt})}, \quad (2)$$

where  $P_E$  is the Euler buckling load determined by Eq. (1);  $A_g$  is the net section area of the FRP member;  $K_s$  is the shear parameters related to the shape of the cross section, for rectangular section and circular section which is 0.83 and 0.9 respectively.

Zureick et al [8,9] had an experimental study on GFRP square pipes under axial compression. The section of the specimens was a 76.2 mm × 76.2 mm square with the wall of thickness of 6.3 mm. Their slenderness ratios were 89, 87, 76, and 66 respectively. It was found that the buckling load of the experimental results corresponded well with the results of the modified Euler formula. Zureick and Scott [9] conducted experimental studies on two types of wide flange H-shaped section and 2 types of box-section GFRP components under axial compression. Each type of section included 6 specimens, totally 24 specimens. Their effective slenderness ratios were from 36 to 103. The ratios between the experimental results and the calculated results by Eqs. (1) and (2) are 0.85–0.97 and 0.88–1.01 respectively. Hence, the reduction factor of 0.85 on the basis of the buckling load by Eq. (2) was proposed for design of GFRP component under axial compression.

Barbero et al [10,11] studied the buckling properties of the FRP components under the coupling influence of overall buckling and local buckling.

It is indicated that the influence of initial geometric defect and initial eccentricity were not considered in the previous formulas of the buckling load of FRP members under axial compression. But it is certain that the initial geometric defect and initial eccentricity exist in real structures for different reasons. Therefore, a modified Perry formula [12] to calculate the buckling load of the GFRP member is suggested based on fitting tested members to obtain the equivalently relatively initial bending  $\varepsilon_0$ . The formula is

$$\begin{cases} \varphi = \frac{1}{2\lambda^2} \left[ (1 + \varepsilon_0 + \lambda^2) - \sqrt{(1 + \varepsilon_0 + \lambda^2)^2 - 4\lambda^2} \right], \\ P_{cr} = \varphi f_L A \end{cases} \quad (3)$$

where  $\varphi$  is stability factor;  $P_{cr}$  is the buckling load;  $f_L$  is the longitudinal compressive strength, which should

**Table 3** Comparison of stability factor between calculation and experimental results

equation	$(\varphi_c/\varphi_E)_{\max}$	$(\varphi_c/\varphi_E)_{\min}$	meaning $m$	mean-square deviation $\sigma$	$\sigma/m$ %
modified Euler Eq. (2)	1.60	0.87	1.11	0.17	15.1
modified Perry Eq. (6)	1.43	0.76	1.04	0.14	13.5

be 198.4 MPa for GFRP pipes used according to the experimental results in Table 1, and  $\bar{\lambda}$  is the regularized slenderness ratio, which is

$$\bar{\lambda} = \frac{\lambda}{\pi} \sqrt{\frac{f_L}{E_L}}, \quad \lambda = \frac{\mu L}{r}, \quad r = \sqrt{\frac{I}{A}}, \quad (4)$$

where  $E_L$  is the longitudinal elastic modulus of the GFRP component;  $I$  is the sectional moment of inertia;  $A$  is the section area of components;  $r$  is the sectional gyration radius;  $\mu$  is the effective length coefficient of the component.

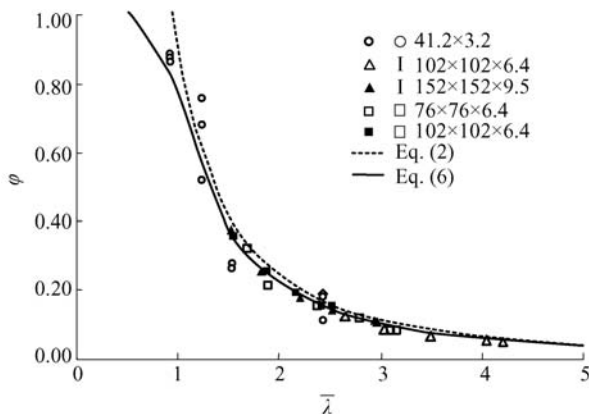
Refer to The Technical Code of Cold-Formed Thin-Wall Steel Structures [13], the expression of initially relative eccentric ratio is

$$e_0 = a + b\bar{\lambda}^2. \quad (5)$$

Fitting the experimental data and the literature data [9] using the least square method, the result of  $a$  is  $-0.04$ ,  $b$  is  $0.09$ . Substituting to Eqs. (3) and (5), then,

$$\varphi = \frac{1}{2\bar{\lambda}^2} \left[ (0.96 + \bar{\lambda}^2) - \sqrt{(0.96 + 1.09\bar{\lambda}^2)^2 - 4\bar{\lambda}^2} \right]. \quad (6)$$

As the consequence, Eq. (6) has a better corresponding with the test data than Eq. (2) as comparing in Table 3. The calculated results of Eqs. (2) and (6) and the test data are illustrated in Fig. 9. It can be seen that Eq. (2) may over-estimated the buckling load of the members with the smaller slenderness ratio so as to acquire an unsafe design.

**Fig. 9** Stability factor curve of FRP member under axial compression

Therefore, Eq. (6) should be used to determine the stability factor of the FRP members. In practical design, a reduction coefficient  $\phi_c$  should be multiplied on the results of Eq. (6). According to the analysis based on the test results, the guarantee rate is 97.72%, when it is  $\phi_c = 1/(m + 2\sigma) = 0.75$ .

## 5 Conclusions

1) It is shown in the axial loading test of five short GFRP pipes that they have the characteristics of linear elastic and brittle failure. And the dispersion of the compressive strength of GFRP is considerable, the maximum variation coefficient reaches 20%, but the dispersion of its elastic constant is smaller relatively as its variation coefficient is within 6%.

2) Based on the experimental study of long GFRP pipes with the different slenderness ratio, the relationships of axial load to lateral displacement, vertical displacement and strain are obtained. It was found that the pipes with smaller slenderness ratio can be compressed to fracture at the ultimate strain caused by obvious lateral deformation after buckling, whereas, the pipes with larger slenderness ratio buckle in elastic and fail in oversize deformation.

3) Based on the test results in this paper and literature, a stability factor formula of GFRP members under axial compression is presented, in which the initial defect and eccentricity are considered. And a calculation method for design buckling strength is proposed.

**Acknowledgements** This work was supported by the National Natural Science Foundation of China (Grant No. 50238030).

## References

- Ye Lieping, Feng Peng. Applications and development of fiber-reinforced polymer in engineering structures. China Civil Engineering Journal. 2006, 39(3): 24–36 (in Chinese)
- Shen Guanlin. Composites Mechanics. Beijing: Tsinghua University Press, 1996 (in Chinese)
- Zhang Yulong. Handbook of Advanced Composites Manufacture Technologies. Beijing: China Machine Press, 2003 (in Chinese)
- Berthelot J M. Composite Materials: Mechanical Behavior and Structural Analysis. New York: Springer-Verlag, 1999
- Goodman J W, Gisksman J A. Structural evaluation of long boron composite column. Composite Materials: Testing and Designing, 1969, ASTM STP 460: 460–469
- Hewson P J. Buckling of pultruded glass fibre-reinforced channel section. Composites, 1978, 9(17): 56–60

7. Lee D J, Hewson P J. The use of fiber-reinforced plastics in thin-walled structures. In: Richards T H, Stanley P, eds. *Stability Problems in Engineering Structures and Components*. New York: Elsevier Applied Science, 1978, 23–55
8. Zureick A, Yoon S, Scott D. Experimental investigation on concentrically loaded pultruded columns. In: Hamlin P, Verchery D, eds. *Proceedings of 2nd International Symposium of Textile Composites in Building Construction*. Paris: 1992, 207–215
9. Zureick A, Scott D. Short-term behavior and design of fiber-reinforced polymeric slender members under axial compression. *Journal of Composites for Construction*, 1997, 1(4): 140–149
10. Barbero E J, Raftoyiannis I G. Euler buckling of pultruded composite columns. *Composite Structures*, 1993, 24(2): 139–147
11. Barbero E J, Tomblin J. A phenomenological design equation for FRP columns with interaction between local and global buckling. *Thin-Walled Structures*, 1994, 18(2): 117–131
12. Chen Ji. *Stability of Steel Structures: Theory and Design*. 2<sup>nd</sup> ed. Beijing: Science Press, 2003 (in Chinese)
13. GB50018-2002 *Technical Code of Cold-Formed Thin-Wall Steel Structures*. 2001 (in Chinese)